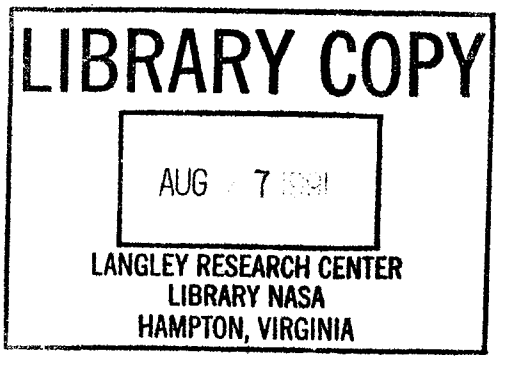

(NASA-CR-174061) A HIGH RESOLUTION SPECTROSCOPIC STUDY OF THE OXYGEN MOLECULE Ph.D. Thesis Final Report (Maryland Univ.) 32 p HC A03/MF A01 CSCL 07D

N85-11150

Unclas G3/25 24425

Final Report for

NASA grant NAG-5-222

A High Resolution Spectroscopic Study of the Oxygen Molecule*

Kenneth J. Ritter

University of Maryland

Institute for Physical Science and Technology

College Park MD.

November 1984

* From a dissertation to be submitted to the Gaduate School, University of Maryland, by Kenneth James Ritter in partial fulfillment of the requirements for the Ph.D. degree in Physics.

Abstract-

A high resolution spectrometer incorporating a narrow line width ($<10\ cm^{-4}$) tunable dye laser has been used to make detailed absorption profiles of 57 spectral lines in the Oxygen A-Band at pressures up to one atmosphere in pure O_2. The observed line profiles are compared the Voigt, and a collisionally narrowed, profile using a least squares fitting procedure. The collisionally narrowed profile is shown to compare more favorably to the observed profiles. Values of the line strengths and self broadening coefficients, determined from the least square fitting process, are presented in tabular form. The distribution of line strengths is compared to expressions given by Childs and Mecke[1], Schlapp[2,3], and Watson[4]. The expression by Watson is found to be in closest agreement with the experimentally determined strengths. The self-broadening coefficients are compared with the measurements of several other investigators.

Background-

The oxygen A-band is an electronic-rotational band of molecular oxygen centered at 13122cm^{-1} in the near infrared. The "A-band" designation was given to this band by early solar spectroscopists who first observed it as an unidentified absorbtion in solar spectra. Several early studies of the band were made in this way[5], using atmospheric slant paths with the sun as a source. These measurements provided accurate line positions[6], and estimates of the line intensities. Using these measurements, Van Vleck[7] and Mulliken[8] were able to show that the A-band is a magnetic dipole transition between the $^3\Sigma_g^-$ ground electronic state and the $^1\Sigma_g^+$ excited state of molecular oxygen. Several bands are produced by this electronic transition, the A-band corresponds to the (0-0) vibrational band of this transition.

The rotational levels of these states are designated by the quantum numbers J and N. The N quantum number refers to the angular momentum of the revolving nuclei. The J quantum number refers to the total angular momentum, which is the sum of the rotation and electron spin angular momentum. The ground state, which has a spin of unity, is split into three levels corresponding to J"=N",N"+1,N"-1 (double primes and single primes denote ground and upper states respectively), the upper electronic level, with S=0, is a singlet state with J'=N'.

The zero nuclear spin of the oxygen atom allows only symmetric states to exist. This, when considered with the electronic and rotational symmetries of the total wave function, requires N" to be odd for the $^3\Sigma_g^-$ ground state and N' to be even for the $^1\Sigma_g^+$ upper state (see Tinkham[9] and Herzberg[10]). This in addition to the familiar dipole selection rule $\Delta J=0,\pm1$ and the requirement that $\Delta s=\Delta J-\Delta N = 0,\pm1$ leads to the following selection rules:

$$\Delta N=\pm1, \Delta J=0,\pm1, \Delta J+\Delta N=0,\pm1$$

The transitions may be written the form $(\Delta N)(\Delta J)N",J"$, where, in accordance with the above selection rules, there are four types of transitions $(\Delta N)(\Delta J)$= PP,PQ,RQ and RR.

Recently, interest in this band has been revived due to its use in laser remote sensing systems which measure atmospheric temperature and pressure.[11-13] For these systems to realize their full potential, accurate spectroscopic information is essential. The currently available values of the line parameters for this band are probably inadequate for this purpose. The previously existing measurements of this band were made using grating spectrometers. These instruments have relatively low resolution, often with an instrumental width on the order of the spectral line width being measured. This, along with the close spacing of lines in this band (($2cm^{-1}$), which complicates high pressure

measurements, was responsible for limiting the accuracy of these earlier measurements. Values for the band strength determined in the most recent laboratory measurements vary by as much as 15% between investigators, while the line widths show even less agreement. For these reasons, the present study was initiated to provide more accurate line parameters, and to make a general high resolution study of line shapes in this band.

Spectrometer Sys tem-

In order to make improved line parameter measurements in this study, a narrow linewidth tunable dye laser was used in conjunction with a multi-pass absorption cell to produce high resolution absorption profiles. The narrow linewidth of the laser ($<10^{-4}$ cm^{-1}) used in this system allows measurements to be made at pressures of an atmosphere and less, where the spectral lines are well separated, without complications introduced by the instrument width.

A diagram of the laser spectrometer system is shown in figure 1. The tunable Coherent model 599 dye laser was operated with a 1.3×10^{-3} molarity solution of oxazine 750 dye in a solvent consisting of 20 parts ethylene glycol to one part propylene carbonate. The dye laser was optically pumped by a 4 watt krypton laser. This dye laser is capable of making continuous scans of up to $1cm^{-1}$ anywhere in the tuning range of the dye. As shown in figure 1, the

laser output was chopped at 1KHz, and directed through the multi-pass absorption cell by the second beamsplitter. The radiation transmitted through the cell was detected by diode 1. The remaining radiation, transmitted through beamsplitter 2 and detected by diode 0, was used as a laser power reference. The output of each diode was synchronously detected by a lock-in amplifier. During a scan, outputs from the lock-in amplifiers along with a scan voltage from the laser were digitized and stored on magnetic tape for later analysis.

Two scans were used to produce each completed absorption profile. One, a background scan, was made with the absorption cell evacuated. A second, the absorption scan, was made with the cell filled to a specific pressure. For each scan, the ratio between the sample cell channel (diode 1) and the laser power channel (diode 0) was taken at each point. A completed scan was then produced by taking the ratio of the absorption scan with its respective background scan. In practice, only one background scan was necessary for each series of scans on a specific line. This procedure produced low noise absorption spectra while minimizing distortions due to laser power fluctuations and frequency dependent transmission of windows, beamsplitters and other optical elements. Figure 2 is a series of absorption spectra (of the PQ 15,14 line) produced by this system.

The air paths between the laser and the two detectors were set equal and as short as possible (approximately 1

meter). This was done so that the effects of weak atmospheric absorption would be eliminated when the ratio between the two channels was taken. The dye laser cavity and the dye laser reference etalon were purged with nitrogen to prevent distortion of the laser tuning when scanning over an oxygen line. The absorption cell pressure was measured using a MKS Baritron capacitance manometer. This was compared with a similar NBS calibrated pressure transducer and found to have an accuracy of 0.5% . All pure O_2 measurements were made using electronic grade O_2 supplied by Scientific Gas Products (purity 99.998%).

The frequency scan voltage, which was used to provide a frequency scale for the absorption scans, was taken from the voltage drop across the laser's 25Ω temperature-regulated reference resistor[19]. This voltage is proportional to the current which drives the laser frequency tuning system. The relation between this scan voltage and the actual laser tuning was found to be slightly non-linear. To correct this, scans were made of a 10 cm Fabry-Perot cavity.

From these scans, the laser's tuning calibration was found to be well characterized by

$$\Delta\nu = \frac{\nu}{\nu_c}\, a(1+bv^2)v$$

where:

$$a \cong 5.9*10^{-2}\ cm^{-1}/volt$$

$$b \cong -3.7*10^{-4}\ volt^{-3}$$

V = scan voltage (-8 volts $\leq v \leq 8$ volts)

ν = laser frequency

ν_c = calibration frequency

The constant "a" in the calibration was determined from spectra of the RQ(13,14) and RR(15,15) pair of lines, which are seperated by 0.749 cm^{-1} [20]. These lines were scanned several times at the start of each data collection session as a continuing check of the laser's tuning calibration. The rms deviation in the measured seperation of these lines over the entire data collection period (approx. 5 months) was 0.1% .

Data Analysis-

For the self broadening measurements, scans were made of all lines from J"= 1 to 28 in both branches. From four to 13 scans were made of each spectral line at pressures from 30 torr to 800 torr. Each scan consisted of 500 equally spaced points over 0.5cm^{-1}. The laser was tuned at a rate of 0.003cm^{-1}/sec, with lock-in amplifier time constants of 125msec. Line parameters were determined for each scan by non-linear least squares fitting analysis. This consisted of fitting the measured absorption cross-section (K_ℓ) to a calculated absorption cross-section(K_c).

Where: $K_\ell(\Delta\nu) = \frac{-1}{nL} \ln\left(\frac{T(\Delta\nu)}{m\Delta\nu + b}\right)$

$$K_c(\Delta\nu) = \sqrt{\frac{\ln 2}{\pi}} \sum_i \frac{S_i}{\gamma_{D_i}} P(x_i, y_i, \eta_i)$$

$T(\Delta\nu)$ = the measured transmission
$\Delta\nu$ = the laser frequency offset (cm^{-1})
n = number density of absorbers ($molec/cm^3$)
L = path length (cm)
m,b = baseline slope and intercept
S_i = strength of the i^{th} line

γ_{D_i} = Doppler half width of the i^{th} line = $\nu_i\sqrt{\frac{2kT\ln(2)}{mc^2}}$
γ_{L_i} = Lorentz width of the i^{th} line
q_i = Narrowing parameter of the i^{th} line
ν_i = Frequency of the i^{th} line

$$y_i = \sqrt{\ln 2}\,(\gamma_{L_i}/\gamma_{D_i})$$
$$x = \sqrt{\ln 2}\,(\nu - \nu_i)/\gamma_{D_i}$$
$$q = \sqrt{\ln 2}\,(q_i/\gamma_{D_i})$$

$P(x, y, \eta)$ = Line profile function

A Marquardt[21,22] fitting procedure, with all points equally weighted, was used in the least-squares fitting process. Initially, a Voigt profile was used in the fitting process. The Voigt function was calculated using a routine by Humlicek, which calculates the complex function:

$$w(z) = \exp(-z^2) * \mathrm{erf}(-iz)$$

Values produced by our version of this routine[25] were compared with tables of this function[26] to confirm that the program was working properly.

The Voigt function and its derivatives can be calculated using the relations:

$$P(x,y) = Re\{w(x+iy)\}$$
$$w'(z) = -2zw(z) + 2i/\sqrt{\pi}$$

Figure 3 is an example of the typical results found when fitting to the Voigt profile. The upper trace (fig 3a) shows the measured absorption scan, the lower trace (fig 3b) shows (on an expanded scale) the deviation between the fitted and measured absorption functions. The form of the deviation shown here was observed for all of the data scans, with the largest deviation observed at about 300 torr. This type of deviation from a Voigt profile appeared to be consistent with that caused by collisional narrowing effects[28]. Therefore, for further analysis, a profile which includes collisional narrowing was used.

A number of line profile functions which include collisional narrowing have been presented in the literature. There were three considerations that went into the selection of a particular profile for use in this study. First, the collisional narrowing observed here is only a small (~1%) correction to the Voigt profile. Since all of the collisionally narrowed profiles reduce to a Voigt profile, the particular model isn't an overriding

concern for small corrections. A second consideration was that all of the profiles observed in this study were symmetric, which eliminated all assymetric profile functions from consideration. The final consideration was that fast numerical calculation of the profile was required.

All of these requirements are met by Rautian's[17] hard collision model for the case of statistical independence between phase changing and velocity changing collisions. This profile is given by the expression:

$$P(x,y,\eta) = Re\left\{\frac{w(x+i[y+\eta])}{1-\sqrt{\pi}\,w(x+i[y+\eta])}\right\}$$

This function, used with Humlicek's routine for w(z), provides for simple and fast numerical evaluation of the line profile and its derivatives.

Figure 3c shows the deviation between the fitted absorption cross-section, using the narrowed profile, and the experimentally determined absorption cross-section function. Figure 3 clearly shows that the collisionally narrowed profile fits the observed profile significantly better than the Voigt profile does. Similar results were observed for all the data scans except at low presures (P<75 torr). At this pressure and below, both functions fit the observations. Presumably, the Voigt function would also fit the observations at high pressures. However, at 1 atm

which was the highest pressure used in this study, the Rautian function still fit the data better than the Voigt function.

Figure 4 shows the narrowing parameter verse pressure. The points included in this plot are for the best 30% of the data as determined by the uncertainties estimated in the fitting routine using a standard error estimation method.[29] Examination of all of the points at a particular pressure (in fig. 4) revealed no observable J" dependence in the narrowing parameter. This is expected for collisional narrowing, since the narrowing process depends only on the change in molecular motion caused by collisions, and not on the internal state of the molecule. The curve through the points is the result of a least-square fit to a quadratic. Since the narrowing parameter is the effective frequency for velocity changing collisions, it is expected to be proportional to the pressure. The results here indicate that the ratio of narrowing parameter to pressure increases with pressure. Pine[30] has found a similar result for collisional narrowing in HF when using the same line profile as used here. Since this is difficult to explain theoretically, and may indicate that the hard collision model assumed by this line function is not strictly valid in this case, we will, for the present, take the the expression for the narrowing parameter as an empirical relationship.

Analysis of Self-Broadening Coefficients-

The self-broadening coefficient for each transition was determined from the width parameters produced by the least-squares fitting process. The widths for each transition were fit (as a function of pressure) to a line, the slope of which was then taken as the broadening coefficient. Figure 5 shows the width of the PQ 15,14 transition at several pressures, along with the line used to determine the broadening coefficient. The widths determined for the Voigt and Rautian line profile functions were slightly different. The broadening coefficients were about 1% less for the Voigt results than for the Rautian results. Also, the Voigt width vs pressure curves had a small but noticable negative intercept of approximately $W(P=0)=-0.0003cm^{-1}$.

Table I lists the values determined for the self-broadening coefficients of each line (using the Rautian profile). Figure 6 shows the self-broadening coefficients graphically as a function of J". The error bars on each point (and those listed in table I) are the estimated errors in the slope of the width vs pressure lines, determined using a standard error estimation technique[29]. Also shown in figure 6, are the results of self-broadening measurements reported by other investigators. The present measurements indicate that, to within the accuracy of the measurements, pairs of lines in

each branch which have the same K" values have the same width. Significant differences between the widths of these pairs is seen only at low J" (J"<5), and these differences increase toward lower J". None of this structure is apparent in the previous measurements.

TABLE I. Self Broadening Coefficients of Oxygen A-band Transitions

LINE	broadening coefficient cm^{-1}/atm	standard deviation
PP 1, 1	0.05892	0.00016
PQ 3, 2	0.05571	0.00030
PP 3, 3	0.05522	0.00011
PQ 5, 4	0.05305	0.00019
PP 5, 5	0.05279	0.00013
PQ 7, 6	0.05098	0.00008
PP 7, 7	0.05078	0.00008
PQ 9, 8	0.04922	0.00013
PP 9, 9	0.04926	0.00008
PQ 11,10	0.04801	0.00010
PP 11,11	0.04814	0.00014
PQ 13,12	0.04716	0.00016
PP 13,13	0.04697	0.00019
PQ 15,14	0.04581	0.00002
PP 15,15	0.04581	0.00014
PQ 17,16	0.04506	0.00015
PP 17,17	0.04417	0.00005
PQ 19,18	0.04321	0.00024
PP 19,19	0.04317	0.00021
PQ 21,20	0.04169	0.00031
PP 21,21	0.04132	0.00017
PQ 23,22	0.04028	0.00015
PP 23,23	0.04022	0.00024
PQ 25,24	0.03883	0.00019
PP 25,25	0.03946	0.00018
PQ 27,26	0.03774	0.00026
PP 27,27	0.03783	0.00058
PQ 29,28	0.03553	0.00037
PP 29,29	0.03535	0.00049

TABLE I (cont.)

LINE	broadening coefficient cm^{-1}/atm	standard deviation
RR 1, 1	0.06064	0.00036
RQ 1, 2	0.05707	0.00017
RR 3, 3	0.05434	0.00014
RQ 3, 4	0.05364	0.00015
RR 5, 5	0.05135	0.00027
RQ 5, 6	0.05115	0.00020
RR 7, 7	0.04983	0.00014
RQ 7, 8	0.04924	0.00009
RR 9, 9	0.04861	0.00018
RQ 9,10	0.04838	0.00018
RR 11,11	0.04726	0.00012
RQ 11,12	0.04736	0.00019
RR 13,13	0.04598	0.00017
RQ 13,14	0.04594	0.00016
RR 15,15	0.04477	0.00015
RQ 15,16	0.04444	0.00015
RR 17,17	0.04340	0.00022
RQ 17,18	0.04331	0.00025
RR 19,19	0.04199	0.00011
RQ 19,20	0.04215	0.00013
RR 21,21	0.04067	0.00010
RQ 21,22	****	****
RR 23,23	0.03937	0.00023
RQ 23,24	0.03926	0.00021
RR 25,25	****	****
RQ 25,26	0.03776	0.00030
RR 27,27	0.03721	0.00051
RQ 27,28	0.03788	0.00030
RR 29,29	0.03253	0.00053
RQ 29,30	0.03195	0.00045

Analysis of Line Strengths -

Strengths for each transition were determined by taking the simple average of the strength parameter values determined for each scan of that transition by the least-squares fitting process. As with the self-broadening coefficients, the strengths determined from the Voigt profile analysis were about 1% less than those determined using the Rautian profile. Values for the line strengths are listed in table II, and shown in graphical form in figure 7. The third column in table II contains the calculated values for the line strengths.

The strength of an absorption line may be written as:[31]

$$S_{J''} = \frac{C_B \nu_{J''} f(J'')}{Q(T)} \exp\left(-hcE''/KT\right)$$

where: $\nu_{J''}$ = center frequency of the line

$Q(T)$ = rotational partition function

E'' = ground state energy level

C_B = band cross-section

$f(J'')$ = weighting factor

h,c,k,T = standard meanings

The band cross-section C_B, which is related to the band strength, can be determined from the measured line strengths all other quantities are well known except for the weighting function $f(J'')$. The weighting function is

TABLE II. Comparison of observed and calculated strengths using the Watson weighting function

Cross-section: C= 1.735E-026 +- 1.7E-028 cm^2/molec
Band Strength: B= 2.275E-022 +- 2.3E-024 cm^{-1}/(molec/cm^2)

All strengths were corrected to 294.0 degrees Kelvin

LINE	Obs. Strength [cm^{-1}/(molec/cm^2)]	Calc Strength [cm^{-1}/(molec/cm^2)]	% Dev (obs-calc)/obs
PP 1, 1	3.156E-024 +- 0.56%	3.147E-024	0.29
PQ 3, 2	3.972E-024 +- 0.82%	3.986E-024	-0.35
PP 3, 3	5.890E-024 +- 0.16%	5.863E-024	0.46
PQ 5, 4	6.103E-024 +- 0.27%	6.113E-024	-0.18
PP 5, 5	7.825E-024 +- 0.49%	7.744E-024	1.02
PQ 7, 6	7.283E-024 +- 0.09%	7.258E-024	0.34
PP 7, 7	8.648E-024 +- 0.40%	8.596E-024	0.60
PQ 9, 8	7.467E-024 +- 0.54%	7.417E-024	0.66
PP 9, 9	8.478E-024 +- 0.14%	8.455E-024	0.27
PQ 11,10	6.816E-024 +- 0.62%	6.787E-024	0.43
PP 11,11	7.585E-024 +- 0.39%	7.548E-024	0.50
PQ 13,12	5.659E-024 +- 0.51%	5.666E-024	-0.11
PP 13,13	6.203E-024 +- 0.28%	6.193E-024	0.17
PQ 15,14	4.410E-024 +- 0.07%	4.360E-024	1.13
PP 15,15	4.725E-024 +- 0.32%	4.706E-024	0.40
PQ 17,16	3.149E-024 +- 0.59%	3.114E-024	1.12
PP 17,17	3.334E-024 +- 0.38%	3.328E-024	0.18
PQ 19,18	2.091E-024 +- 0.62%	2.073E-024	0.88
PP 19,19	2.201E-024 +- 0.59%	2.198E-024	0.14
PQ 21,20	1.296E-024 +- 0.62%	1.290E-024	0.48
PP 21,21	1.367E-024 +- 0.70%	1.359E-024	0.61
PQ 23,22	7.614E-025 +- 0.56%	7.518E-025	1.25
PP 23,23	7.939E-025 +- 0.73%	7.882E-025	0.72
PQ 25,24	4.161E-025 +- 0.45%	4.113E-025	1.15
PP 25,25	4.337E-025 +- 0.84%	4.294E-025	1.01
PQ 27,26	2.120E-025 +- 1.46%	2.115E-025	0.26
PP 27,27	2.214E-025 +- 0.29%	2.199E-025	0.66
PQ 29,28	1.019E-025 +- 1.18%	1.023E-025	-0.40
PP 29,29	1.082E-025 +- 1.27%	1.060E-025	1.96
PQ 31,30	****	4.658E-026	****

TABLE II. (cont.)

LINE	Obs. Strength [$cm^{-1}/(molec/cm^2)$]	Calc Strength [$cm^{-1}/(molec/cm^2)$]	% Dev (obs-calc)/obs
RR 1, 1	1.575E-024 +- 0.28%	1.574E-024	0.08
RQ 1, 2	3.648E-024 +- 0.34%	3.668E-024	-0.55
RR 3, 3	4.361E-024 +- 0.61%	4.404E-024	-0.98
RQ 3, 4	6.364E-024 +- 0.44%	6.389E-024	-0.40
RR 5, 5	6.386E-024 +- 0.30%	6.469E-024	-1.30
RQ 5, 6	8.166E-024 +- 0.28%	8.246E-024	-0.98
RR 7, 7	7.515E-024 +- 0.62%	7.545E-024	-0.40
RQ 7, 8	9.051E-024 +- 0.49%	9.049E-024	0.02
RR 9, 9	7.605E-024 +- 0.27%	7.640E-024	-0.46
RQ 9,10	8.805E-024 +- 0.70%	8.843E-024	-0.43
RR 11,11	6.900E-024 +- 0.23%	6.952E-024	-0.76
RQ 11,12	7.813E-024 +- 0.76%	7.861E-024	-0.62
RR 13,13	5.731E-024 +- 0.25%	5.783E-024	-0.91
RQ 13,14	6.423E-024 +- 0.64%	6.433E-024	-0.15
RR 15,15	4.419E-024 +- 0.32%	4.440E-024	-0.49
RQ 15,16	4.855E-024 +- 0.86%	4.879E-024	-0.51
RR 17,17	3.123E-024 +- 0.64%	3.166E-024	-1.40
RQ 17,18	3.379E-024 +- 1.03%	3.447E-024	-2.00
RR 19,19	2.077E-024 +- 1.38%	2.105E-024	-1.35
RQ 19,20	2.246E-024 +- 0.27%	2.275E-024	-1.29
RR 21,21	1.285E-024 +- 0.32%	1.309E-024	-1.92
RQ 21,22	****	1.406E-024	****
RR 23,23	7.608E-025 +- 0.70%	7.629E-025	-0.27
RQ 23,24	8.071E-025 +- 0.35%	8.152E-025	-1.00
RR 25,25	****	4.173E-025	****
RQ 25,26	4.398E-025 +- 1.11%	4.440E-025	-0.96
RR 27,27	2.171E-025 +- 1.32%	2.146E-025	1.18
RQ 27,28	2.344E-025 +- 2.13%	2.275E-025	2.94
RR 29,29	1.051E-025 +- 1.20%	1.038E-025	1.27
RQ 29,30	1.069E-025 +- 2.85%	1.097E-025	-2.58

proportional to the square of the dipole moment operator for a particular transition. In this case the form of this function is dependent on the coupling of the electron spin to the molecular axes. For oxygen this coupling is intermediate between Hund's type a and type b. In type a coupling, the spin is parallel to the internuclear axis, and in type b the spin is parallel to the rotational axis of the molecule. Several expressions for the weighting function have appeared in the literature. The first, due to Childs and Mecke[1], was empirically determined from atmospheric measurements of the A-band. Schlapp[2,3] derived an expression which neglects the coupling of the spin to the rotation axis and includes the spin coupling to the internuclear axis only for the three cases:

$$\lambda/B = 0,\ 4/3,\ 2$$

where:

$$B = \hbar^2/8\pi I$$

λ = the spin-spin coupling constant

For oxygen, $\lambda/B \simeq 1.38$, so Schlapp's $\lambda/B = 4/3$ case will be used here. A third expression by Watson[4] treats both spin couplings in general for any values of the coupling constants.

The expressions for the weighting function $f(J'')$ are summarized in table III. The three sets of expressions are

TABLE III
Weighting functions

Transition	Childs and Mecke[1]	Schlapp[3] (/B=4/3)	Watson[4]
PQ	(J"+1/2)/2	(J"+3/4)/2	C_J*(2J"+1)/2
PP	(J"+1)/2	(J"+1)/2	(J"+1)/2
RR	J"/2	J"/2	J"/2
RQ	(J"+1/2)/2	(J"+1/4)/2	S_J*(2J"+1)/2

C_J = [F2(J)-F1(J)]/[F3(J)-F1(J)]
S_J = [F3(J)-F2(J)]/[F3(J)-F1(J)]

Where F1(J),F2(J) and F3(J) are the ground state energy levels in order of increasing energy. The expressions in this table have been rewritten in terms ofthe ground state rotational quantum number J".

identical for the PP and RR transitions, these transitions were shown by Schlapp[3] to be independent of the type of spin coupling. Miller et.al.[16] were able to show that the Childs and Mecke expression did not fit their observed strengths, but that both the Schlapp and Watson expressions produced equally good agreement to within the accuracy of their measurements.

A comparison of the three weigting functions using the results of the present measurements are shown in figures 8-a,b,c. These plots show the deviation between the observed and calculated strengths for each weighting function. The band cross-section C_g was adjusted to give the best fit between observed and calculated strengths for each case. Clearly, the Childs and Mecke function (fig 8a)

does not conform to the observations. The Schlapp and Watson functions show close agreement above J"=8, this is expected since the two functions are nearly identical except at low J". However, a comparison of figures 8b and 8c for J"=2,4,6 shows that the Watson function produces much better agreement with the data than the Schlapp function.

The band cross-section C_β determined from the strength values of table I and using the Watson weighting is:

$$C_\beta = 1.735 * 10^{-26} \text{ cm}^2/\text{molec}$$

The Einstein transition probability, which provides a convenient means for comparison with the results of other studies, can be calculated from the band cross-section (C_β) using:[31]

$$A_{nm} = 8\pi \nu^3 c\, C_\beta\, M\, g_n/g_m$$

where: M = molecular mass
c = speed of light
$g_n/g_m = 3$ (for this band)

The result for the Einstein transition probability for several of the most recent studies of this band are given in table IV.

TABLE IV

Investigator	A (sec^{-1})	Year
Wark and Mercer[31]	0.145	1965
Adiks,Dianov-Klokov[14]	0.082	1968
Burch and Gryvnak[15]	0.085	1969
Miller,Boese,Giver[16]	0.077	1969
Galkin,Zhukove,Mitrofanova[32]	0.073	1972
present study	0.0887	1984

The band strength can be calculated by summing the strengths calculated for each line in the band, with the result from the present measurements:

$$S = 2.28 * 10^{-22} \ cm^{-1}/(molec/cm^2)$$

Conclusion-

The results of a high resolution spectroscopic study of individual absorption lines of the oxygen A-band have been presented. Accurate calculations of atmospheric transmission can be performed using the line strengths given in table II, and the broadening coefficients in table I. For maximum accuracy at and near line centers, the collisionally narrowed profile of Rautian should be used, with the narrowing parameter given by:

$$q = 0.0072 \ cm^{-1}/atm * P + 0.0121 \ cm^{-1}/atm^2 * P^2 \quad (0 \leq P \leq 1atm)$$

References-

1. W.H.J. Childs and R. Mecke, Zeit. f. Physik 68,344 (1931) .

2. R. Schlapp, Phys. Rev. 39, 806 (1932) .

3. R. Schlapp, Phys. Rev. 51, 342 (1937) .

4. J.K.G. Watson, Can. J. Phys. 46,1637 (1968) .

5. H.D. Babcock and L. Herzberg, Astrophys. J. 108, 167 (1948).

6. D.L. Albritton, W.J. Harrop, and A.L. Schmeltekopf, J. Molec. Spectrosc. 46, 103 (1973).

7. J.H. Van Vleck, Astrophys. J. 80, 161 (1934).

8. R.S. Mulliken, Phys. Rev. 32, 880 (1928).

9. M. Tinkham, "Group Theory and Quantum Mechanics", McGraw-Hill, New York, (1964) p.253 .

10. G. Herzberg, "Molecular Spectra and Molecular Structure I. Spectra of Diatomic Molecules", Van Nostrom Co. Inc., New York (1950) p.238 .

11. J. Kalshoven, C.L. Korb, G. Schwemmer and M. Dombrowski Applied Optics 20, 1967 (1981).

12. C.L. Korb and C.Y. Weng, J. Appl. Meteor. 21,1346 (1982).

13. C.L. Korb and C.Y. Weng, Applied Optics 22, 3759 (1983).

14. T.G. Adiks and V.I. Dianov-Klokov, Bull.(Izv),Acad. Sci. USSR Ocean. Phts. 4,605 (1968).

15. D. Burch and D. Gryvnak, Applied Optics 8,1493 (1969).

16. J.H. Miller, R.W. Boese and L.P. Giver, JQSRT 9, 1507 (1969).

17. T. Nakazawa, T. Yamanouchi, and M. Tanaka, JQSRT 27,615 (1982).

18. Operations Manual for Coherent CR-599-21 Scanning Single Frequency Dye Laser.

19. See reference #10, schematic #Do406-255(A) resistor R17. Using the voltage across this resistor makes the frequency calibration independent of the settings on the laser controller.

20. L.S. Rothman, R.R. Gamache, A. Barbe, A. Goldman, J.R. Gillis, L.R. Brown, R.A. Toth, J.M. Flaud, and C. Camy-Peyret, Applied Optics 22, 2247 (1983).

21. D.W. Marquardt, J. Soc. Indust. Appl. Math. 11, 431 (1963).

22. Bevington, Data Reduction and Error Analysis for the Physical Sciences, McGraw-Hill, New York 1969, p.233 .

23. J. Humlicek, JQSRT 21, 309 (1979).

24. J. Humlicek, JQSRT 27, 437 (1982).

25. Humlicek's routine for w(z), which has an accuracy of[ ] was translated into PASCAL for this work. Results from this translated routine were checked against the tables of Faddeyeva and Terentev to ensure that the routine was working properly.

26. V.N. Faddeyeva and N.M. Terentev, "Tables of Values of the Function w(z) for Complex Argument", Pergamon Press, Oxford (1961).

27. S.G. Rautian and I.I. Sobel'man, Soviet Phys. Usp. 9,701 (1967).

28. P.L. Varghese and R.K. Hanson, Applied Optics 23,2376 (1984).

29. A.A. Clifford, "Multivariate Error Analysis" Wiley and Sons, N.Y. 1973

30. A.S. Pine, J. Mol. Spec. 82,435 (1980) .

31. D. Wark and D. Mercer, Applied Optics 4, 839 (1965) .

32. Galkin, Zukove and Mitrofanova, Opt. i. Spectrosk 33, 837 (1972) .

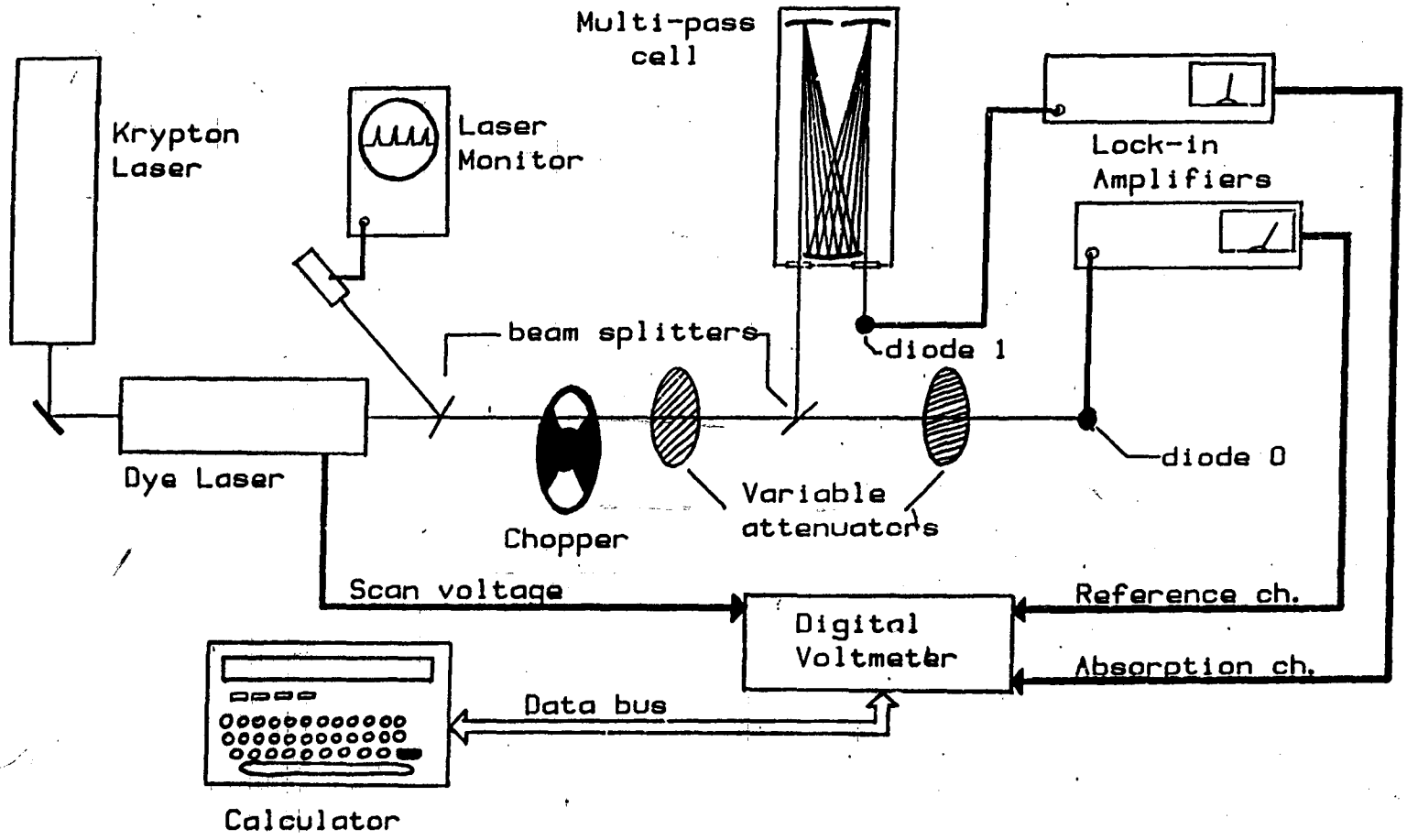

Figure 1. The High Resolution Dye Laser Spectrometer System-
Output from the tunable dye laser is chopped and directed through the multi-pass absorption cell. Part of the output (transmitted through the second beam splitter) is used as a laser power reference. The absorption and reference channels, along with the scan voltage from the laser, are digitized (by the digital voltmeter) and stored on tape by the programmable HP9825 calculator. A pair of variable attenuators is used to adjust intensities on the detectors for maximum dynamic range in both the lock-in amplifiers and the digital voltmeter. The laser monitor is a 0.25cm scanning etalon which is used to monitor the laser mode structure.

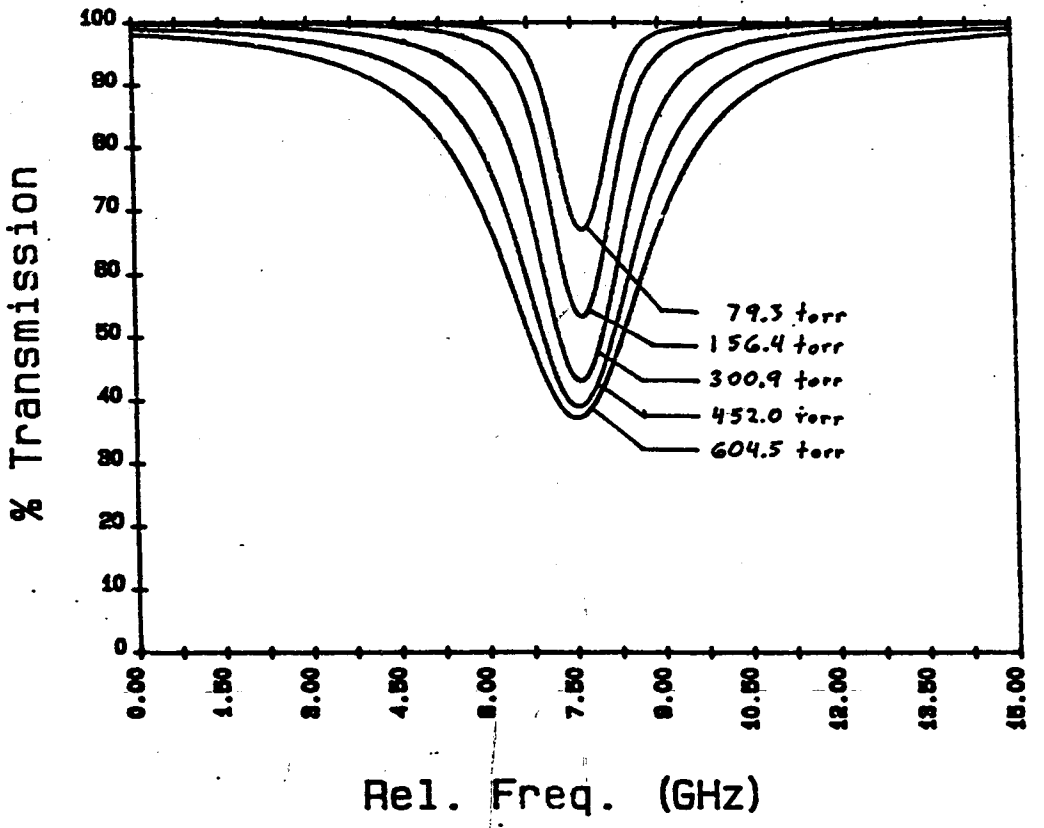

Figure 2. Absorption scans of the PQ 15, 14 line of the oxygen A-band at various pressures of pure oxygen. The path length for this set of scans was 14 meters.

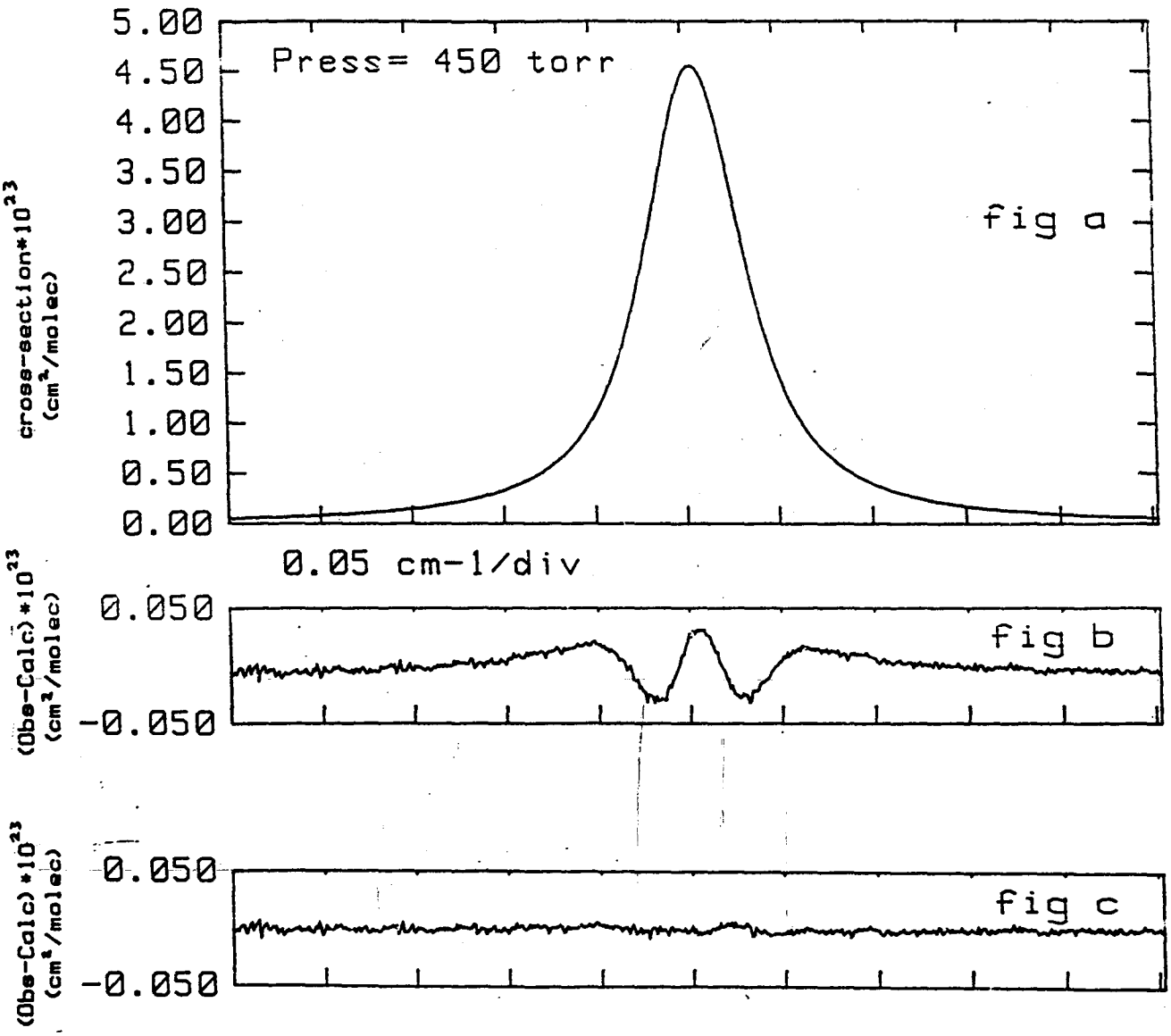

Figure 3. Comparison of Voigt and Rautian profiles to the observed line shape. The upper trace (fig. 3a) shows the measured line profile. The second trace (fig. 3b) shows the deviation between the observed profile and the best-fit Voigt profile. The bottom trace (fig. 3c) shows the deviation between the observed profile and the best-fit Rautian profile.

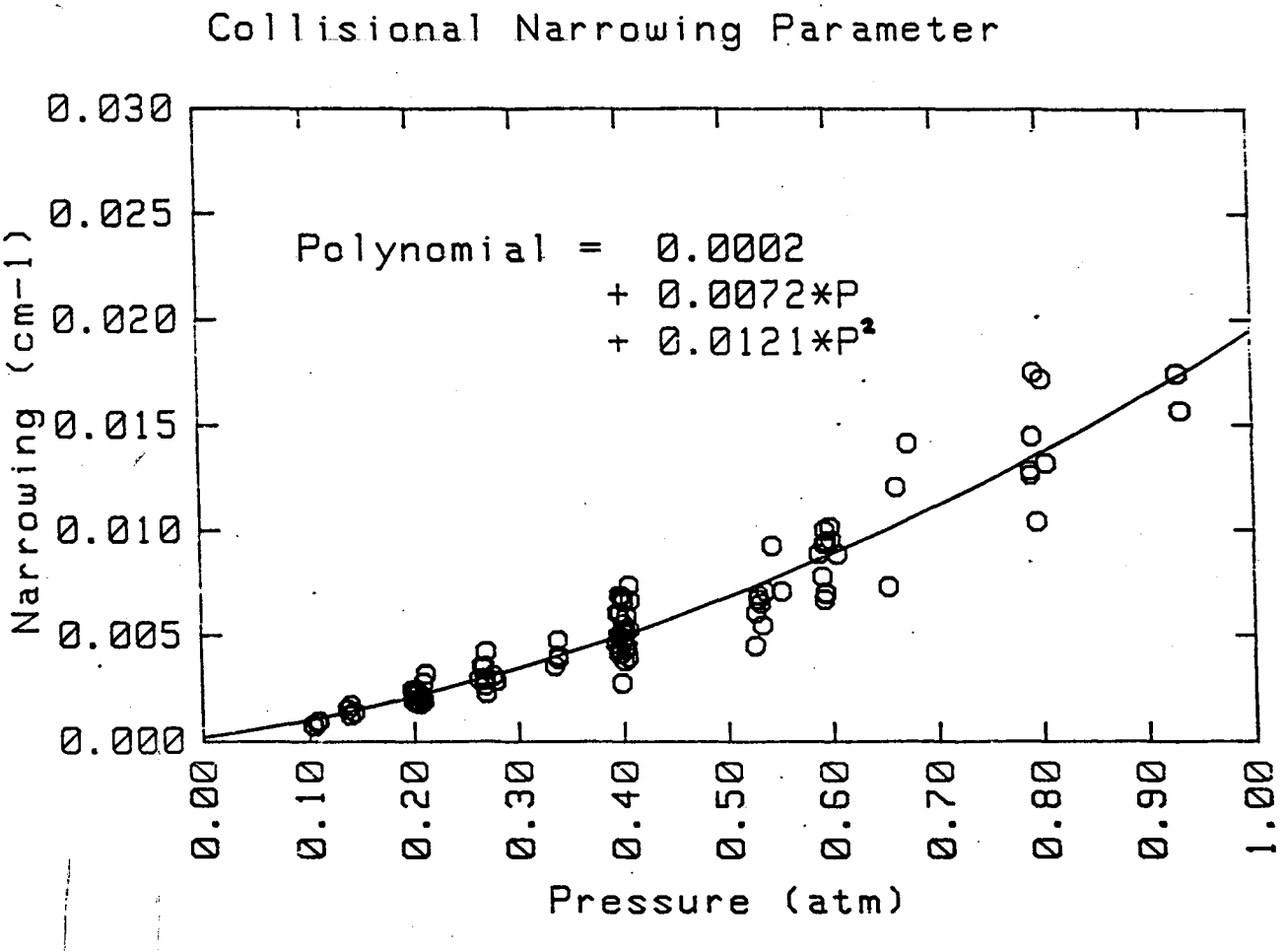

Figure 4. Values of the colisional narrowing parameter for the 30% of the data with the highest signal to noise ratio. The narrowing parameters were determined from least squares fitting to the Rautian collisionally narrowed profile. The polynomial drawn through the points was determined by a least-squares fit to the points contained in this graph.

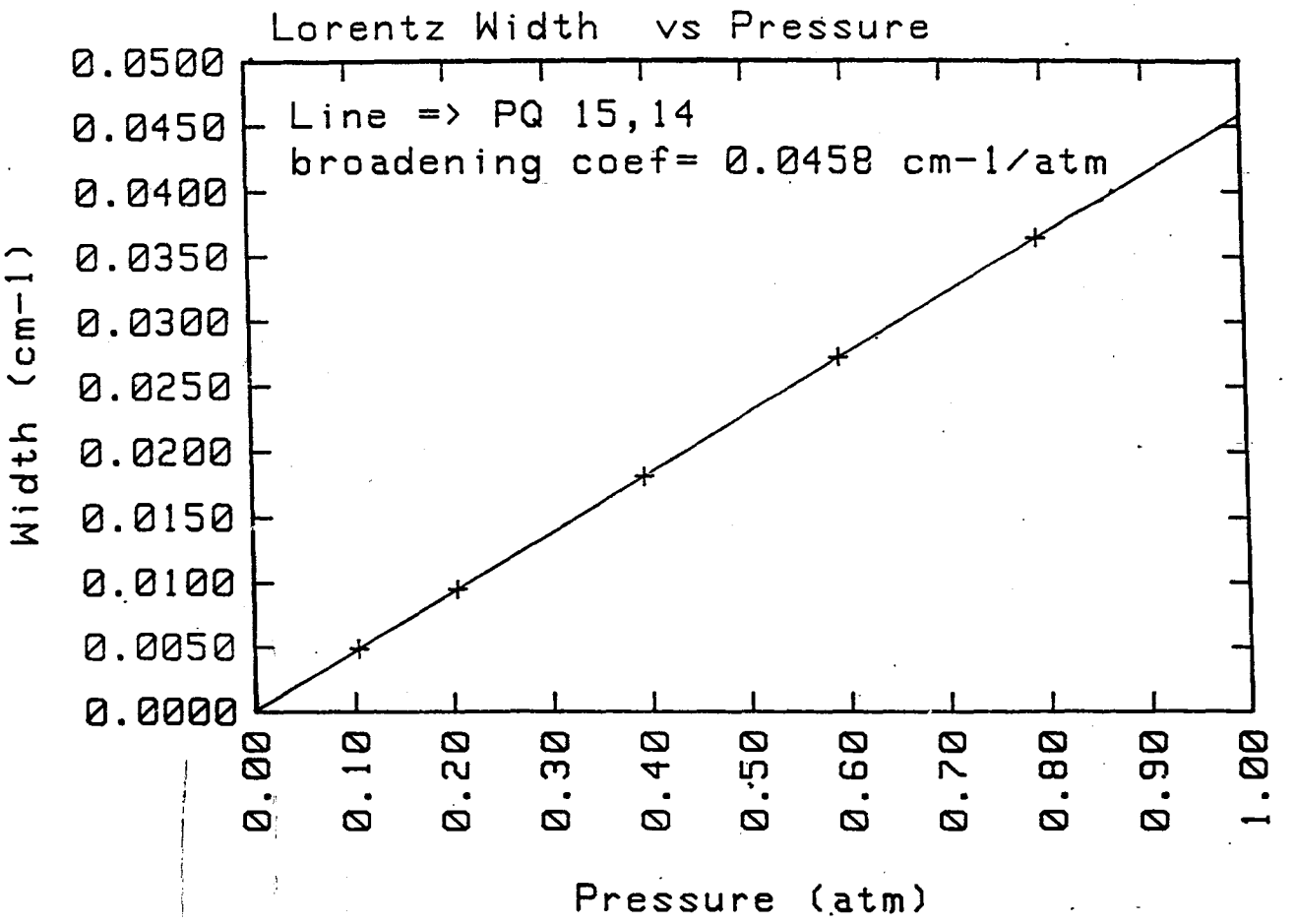

Figure 5. Values of the Lorentz width for the PQ 15.14 line. Widths were determined by least-squares fitting of the Rautian collisionally narrowed profile to the absorption scans shown in figure 2.

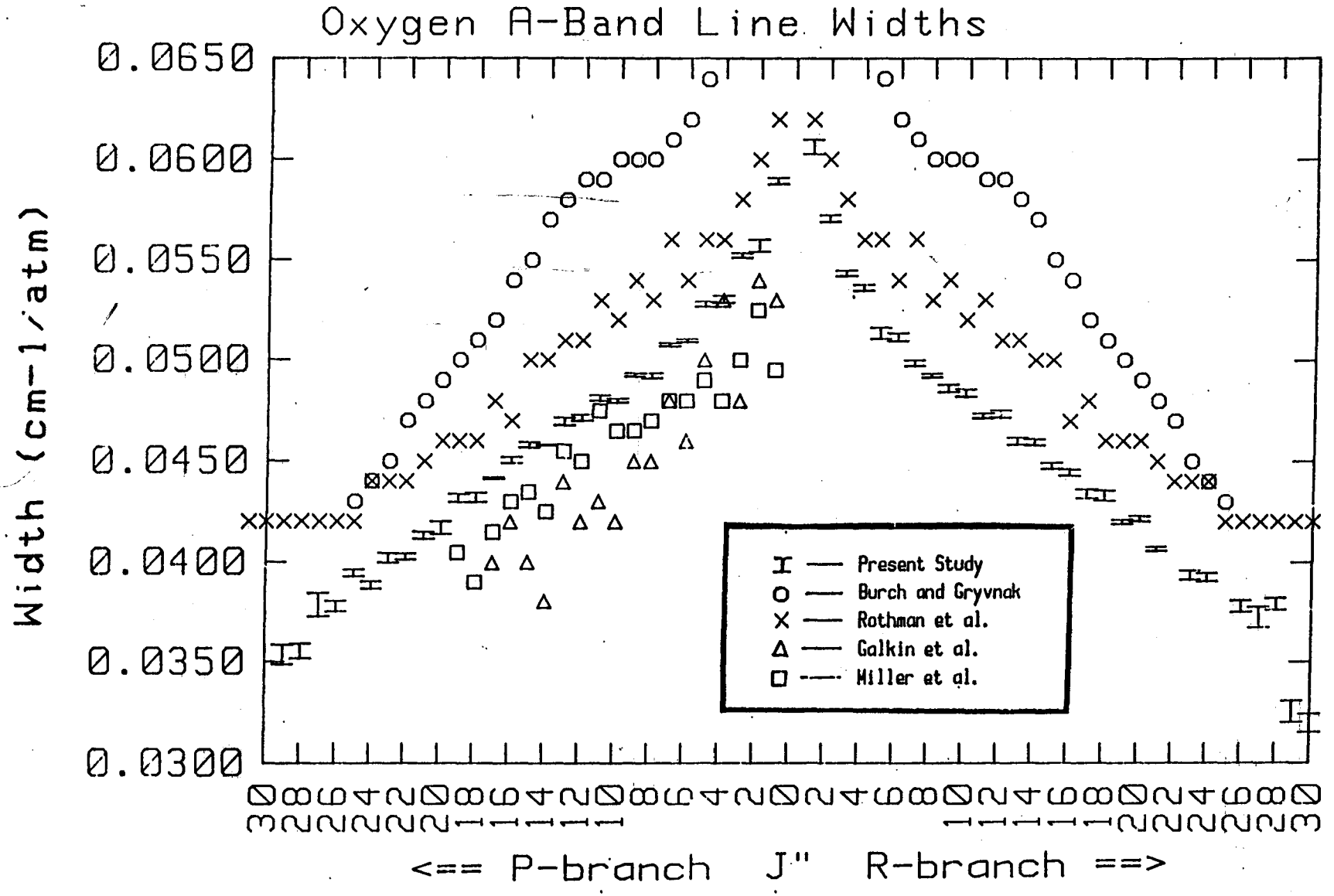

Figure 6. Line widths (self-broadening coefficients). Results from this study and several previously reported studies.

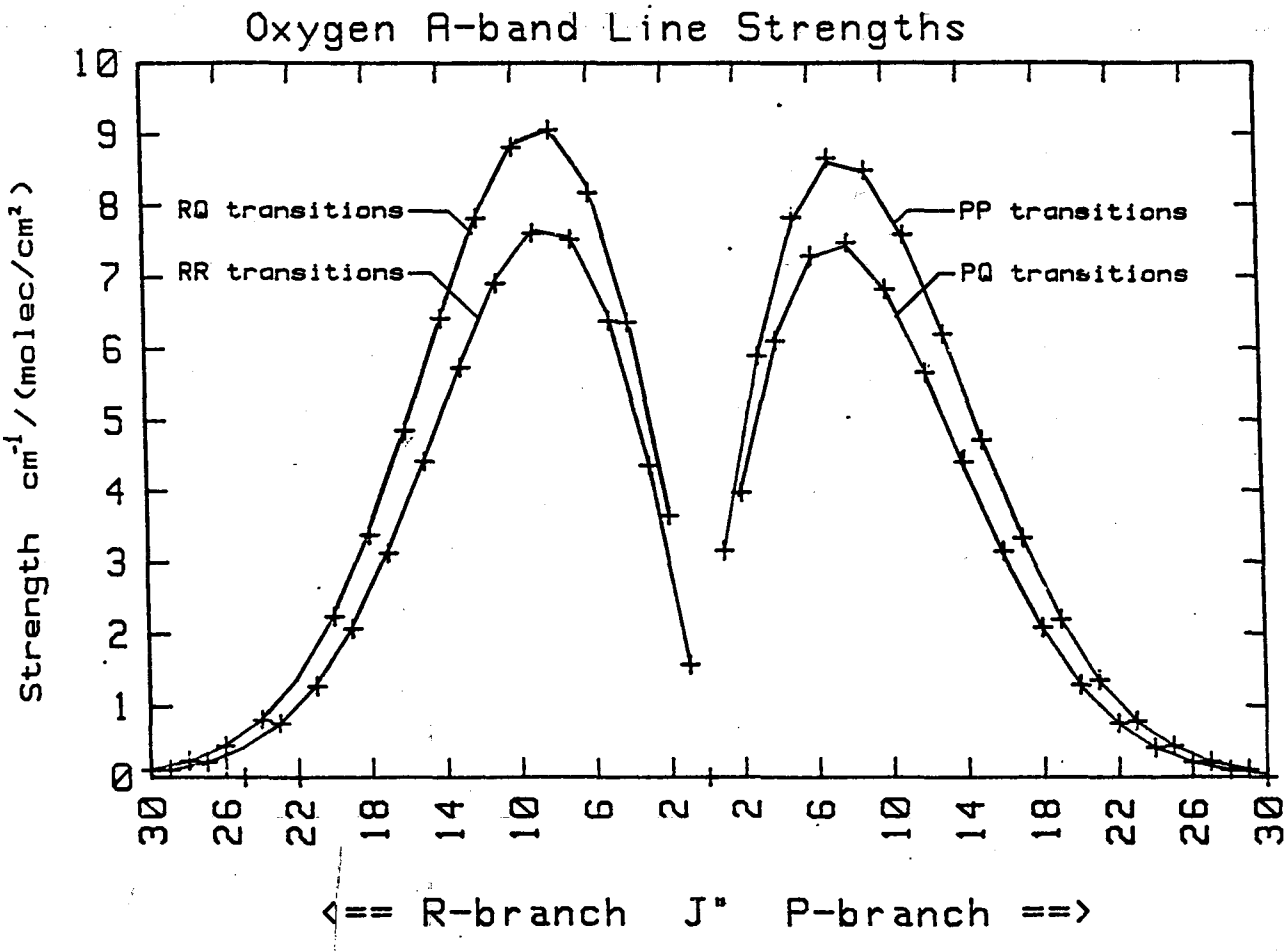
Oxygen A-band Line Strengths
Strength cm⁻¹/(molec/cm²)
RQ transitions
RR transitions
PP transitions
PQ transitions
<== R-branch J" P-branch ==>

Figure 7.

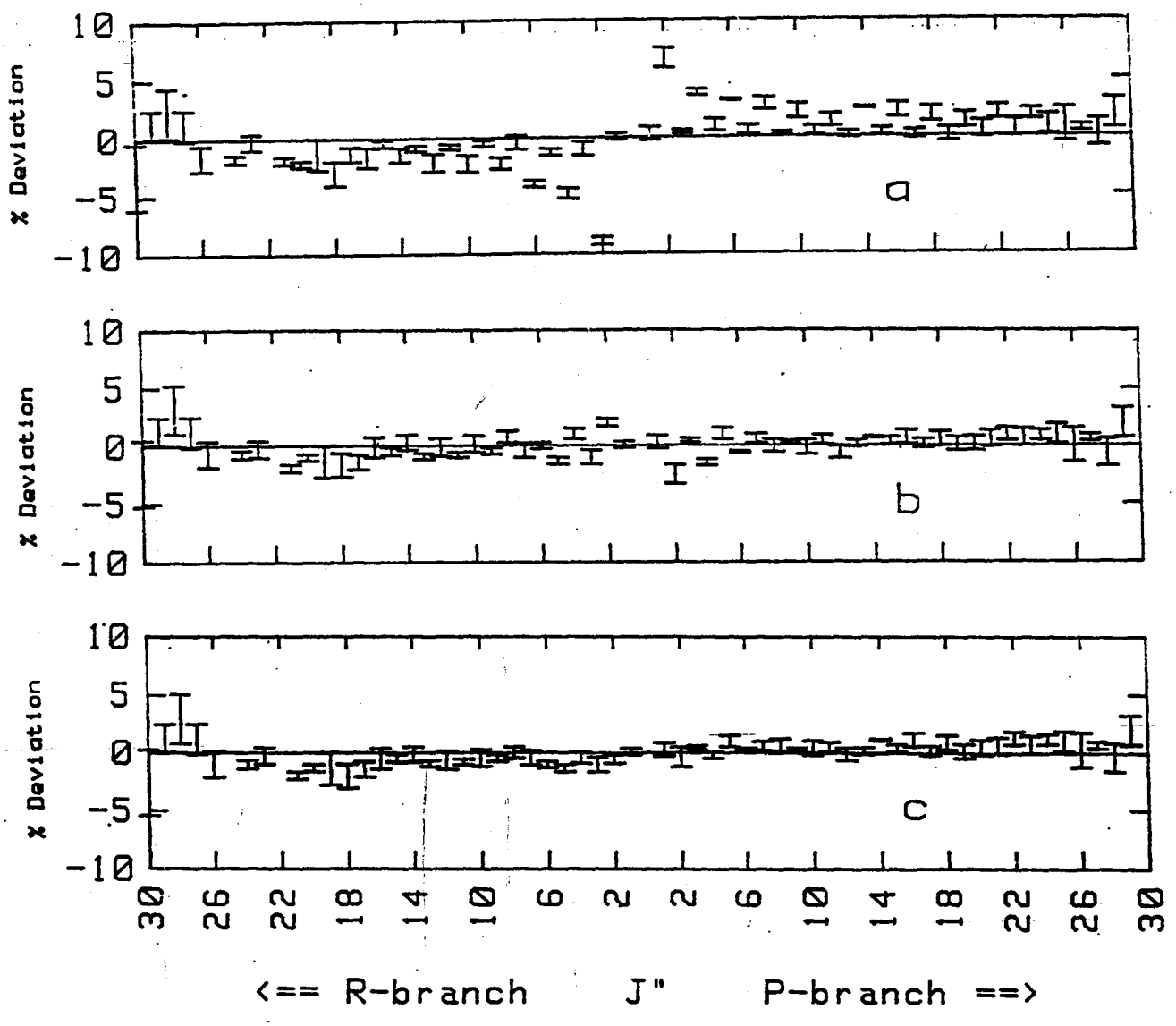

Figure 8. Comparison of weighting functions. Each of these graphs shows the percentage deviation between the observed and calculated line strengths. The three types of weighting functions: Childs and Mecke, Schlapp, and Watson were used for figures 8a, 8b, and 8c respectively. The error bars indicate the standard deviation in the measurements of each line strength.

END

DATE

FILMED

JAN 18 1985